journal

J. Am. Ceram. Soc., 83 [5] 1226–32 (2000)

Experimental Method for Determining Surface Energy Anisotropy and Its Application to Magnesia

David M. Saylor,* Darren E. Mason,† and Gregory S. Rohrer*,‡

Department of Materials Science and Engineering, Carnegie Mellon University, Pittsburgh, Pennsylvania 15213-3890

An experimental technique has been developed to determine the surface energy anisotropy of crystalline solids. The technique is based on atomic force microscopy measurements, which are used to quantify the geometry of thermal grooves, and electron backscattered diffraction pattern measurements, which are used to specify crystallographic orientations. Observations are made at circumferential thermal grooves, where it is assumed that Herring's local equilibrium condition for a triple junction holds and that the grain-boundary energy is independent of its boundary plane. A truncated double Fourier series is used to approximate the surface energy, and the unknown coefficients of the series are determined by fitting the observations to the local equilibrium condition. The method, which should be applicable to most polycrystalline materials, has been tested on magnesia that has been thermally grooved at 1400°C in air. The maximum of the best-fit surface energy function is at (111) and the minimum is at (100). The relative surface energies of the low-index planes are $\gamma_{110}/\gamma_{100} = 1.040 \pm 0.008$ and $\gamma_{111}/\gamma_{100} = 1.072 \pm 0.010$.

I. Introduction

The anisotropy of the surface energy of a crystalline solid can be experimentally evaluated by measuring the geometry of crystallographically indexed surface features. For example, the equilibrium geometries of thermal facets,[1,2] grain-boundary grooves,[3–9] small crystallites,[10,11] and internal cavities[12–14] have been used to deduce relative surface energies. Because these techniques demand either special microstructural features or specimen geometries, each has a limited range of applicability. In this paper, we describe a new technique for determining the anisotropy of the surface energy. The technique involves the analysis of thermal grooves in typical polycrystals, and we illustrate its application by describing a measurement of the surface energy anisotropy of magnesia.

The condition for local equilibrium that relates the geometry of a thermal groove (the dihedral angles at the triple line) and its crystallography (the crystallite orientations) to the energies of the three interfaces was originally described by Herring:[15]

$$\sum_i \gamma_i \mathbf{t}_i + \mathbf{n}_i \frac{\partial \gamma_i}{\partial \beta_i} = 0 \qquad (1)$$

where γ_i is the excess free energy per unit area of the ith interface, $\mathbf{t}_i$ the unit vector that lies in the ith interface and is normal to the line of intersection of the three interfaces ($\mathbf{l}$), $\mathbf{n}_i$ the unit vector normal to the line of intersection such that $\mathbf{n}_i = \mathbf{l} \times \hat{\mathbf{t}}_i$, and β_i the right-handed angle of rotation about $\mathbf{l}$ for the ith boundary measured from a reference direction. Equation (1) represents a force balance and can be separated into two perpendicular components. With reference to Fig. 1, the force balance normal to the macroscopic sample surface (parallel to $\mathbf{e}_3$) is

$$\gamma_3 \cos\alpha - \frac{\partial \gamma_3}{\partial \alpha} \sin\alpha = \gamma_1 \cos\chi_1 - \frac{\partial \gamma_1}{\partial \chi_1} \sin\chi_1 + \gamma_2 \cos\chi_2 - \frac{\partial \gamma_2}{\partial \chi_2} \sin\chi_2 \qquad (2)$$

and the force balance parallel to the macroscopic sample surface is

$$-\gamma_3 \sin\alpha - \frac{\partial \gamma_3}{\partial \alpha} \cos\alpha = \gamma_1 \sin\chi_1 + \frac{\partial \gamma_1}{\partial \chi_1} \cos\chi_1 - \gamma_2 \sin\chi_2 - \frac{\partial \gamma_2}{\partial \chi_2} \cos\chi_2 \qquad (3)$$

The symbols in Eqs. (2) and (3) are defined in Fig. 1. By measuring the geometry and crystallography of thermal grooves, the relative interfacial energies can be determined from the Herring equation. In past thermal groove studies, Eq. (3) has been ignored, and the data analysis has been conducted under the assumption that the torque on the grain boundary is negligible ($\partial\gamma_3/\partial\alpha = 0$).[3–9]

Mykura[3] was the first to extract relative surface energies from an analysis of thermal groove data. The most important feature of Mykura's[3] method is that all of the thermal groove measurements are made at twin boundaries. By measuring only thermal grooves at grain boundaries having the same character, the potentially overwhelming grain-boundary energy anisotropy can be eliminated in such a way that the energies of the free surfaces are the only remaining unknown variables in Eq. (2). Limiting the variations in the grain-boundary energy is the common principle underpinning all subsequent thermal-groove-based surface energy measurements, including the one described in the current paper.

Mykura's[3] method was advanced by Winterbottom and Gjostein,[6,7] who approximated the surface energy as a truncated double Fourier series and used the method of least squares to determine the unknown coefficients of the series that best fitted a set of thermal groove observations. One limitation of Mykura's[3] method is that it can be applied only to the relatively few materials that exhibit a high population of twin boundaries. McLean and co-workers[8,9] devised a more general method involving the characterization of circumferential thermal grooves on the surface of cylindrical wires with a bamboo microstructure. Grooves at different positions around the circumference of the wire are bounded by a range of crystallographically distinct free surfaces, but always have the same grain boundary at the root. Thus, if several hundred thermal groove measurements can be accumulated from a few grain boundaries, Winterbottom and Gjostein's[6,7] fitting method can be used to obtain a series representation of the functional form of the surface energy. Because the methods described above apply only to crystalline materials that twin extensively or can be drawn into wires and recrystallized, they have been applied only to metals such as nickel,[3] copper,[4,8] γ-iron,[5] and gold.[7]

C. A. Handwerker—contributing editor

Manuscript No. 189348. Received May 17, 1999; approved October 21, 1999.

Supported primarily by the MRSEC Program of the National Science Foundation under Award No. DMR-9632556.

*Member, American Ceramic Society.

†Current address: Department of Materials Science and Mechanics, Michigan State University, East Lansing, MI 48864.

‡Author to whom correspondence should be addressed.

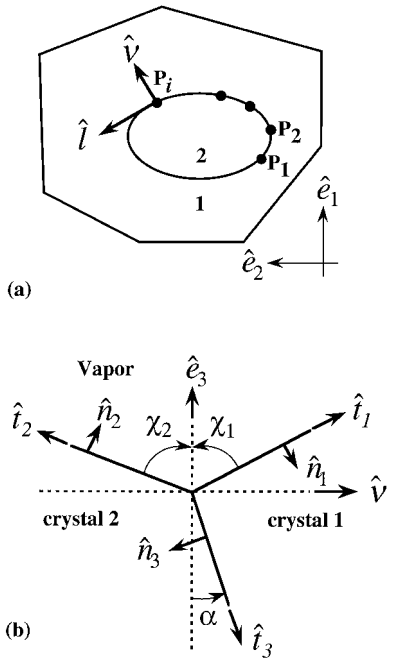

Fig. 1. Coordinate system used for the data analysis. (a) Schematic plane view of an island grain (labeled 2) within a matrix grain (labeled 1). Multiple groove measurements are made around the circumference of the island grain, at points labeled P_i. (b) Schematic cross-section view of a triple junction. Note that **l** points into the plane of the paper.

In the present article, we describe an experimental method that is similar in spirit to those described above but that can be applied to ceramic polycrystals. The only necessary property of the polycrystal is that its microstructure contains a few island grains, or grains enclosed completely or partially by others. The orientation dependence of the surface energy of magnesia at 1400°C has been determined by fitting observations recorded at such grooves to Herring's[15] equilibrium condition. The energy function derived from these data is consistent with observed surface faceting.

II. Experimental Procedure

(1) Experimental Approach

When examining a well-annealed, polycrystalline microstructure, a small grain enclosed within a larger grain is occasionally found. We refer to the smaller, surrounded crystal as an island grain and the larger crystal as the matrix grain. A planar section illustrating this situation is shown schematically in Fig. 1(a); an island grain observed in magnesia is illustrated in Fig. 2. In Fig. 2, the boundary separating the island grain from the matrix grain is easily distinguished by the thermal groove. Assuming that the triple junction at the groove root is in local thermodynamic equilibrium, Eqs. (2) and (3) should then be satisfied at all points, P_i. If the orientations of both grains are determined by backscattered electron diffraction and the inclinations of the three interfaces (defined by χ_1, χ_2, and α) are determined by microscopic analysis at N points along the boundary, then it is possible to specify all of the quantities in Eqs. (2) and (3), except the interface energies and their derivatives. In our analysis, we assume that the vectors defining the interface tangents and normals lie in a single planar section that is perpendicular to the tangent of the triple line.

Determining the surface energy from the N vector equations is a highly nonlinear problem that, because of experimental uncertainties, may not have a classical solution. To determine an approximate form for the surface energy, we make two simplifying assumptions that allow us to arrive at an overdetermined system of linear equations. An approximate solution of these equations then can be found via the method of least squares. First, we assume that the grain-boundary energy is a function only of the misorientation and not the boundary plane. Therefore, $\partial\gamma_3/\partial\alpha = 0$; this is identical to the approximation applied in the earlier work.[3,9] Because the misorientation is fixed at all points across the boundary, the grain-boundary energy (γ_3) is the same in each of the N equations. Second, we use Winterbottom and Gjostein's[6,7] method of approximating the surface energy as a truncated double Fourier series. We have selected the following form for the function:

$$\gamma_s(\theta,\varphi) = 1 + \sum_{i=1}^{R}\sum_{j=0}^{R} \{a_{ij}[\cos(2i\theta) - 1]\cos(j\varphi) + b_{ij}\sin(2i\theta)\cos(j\varphi) + c_{ij}[\cos(2i\theta) - 1]\sin(j\varphi) + d_{ij}\sin(2i\theta)\sin(j\varphi)]\} \quad (4)$$

In Eq. (4), θ and φ are the usual spherical angles, and the energy of the (100) orientation ($\theta = 0$) is normalized to equal 1.0. Using this approximation, the surface energy and its derivatives at each point are determined by the surface orientation and a finite set of unknown coefficients. For a series of order R, the number of coefficients is $2R(2R + 1)$, so that, for a set of N observations

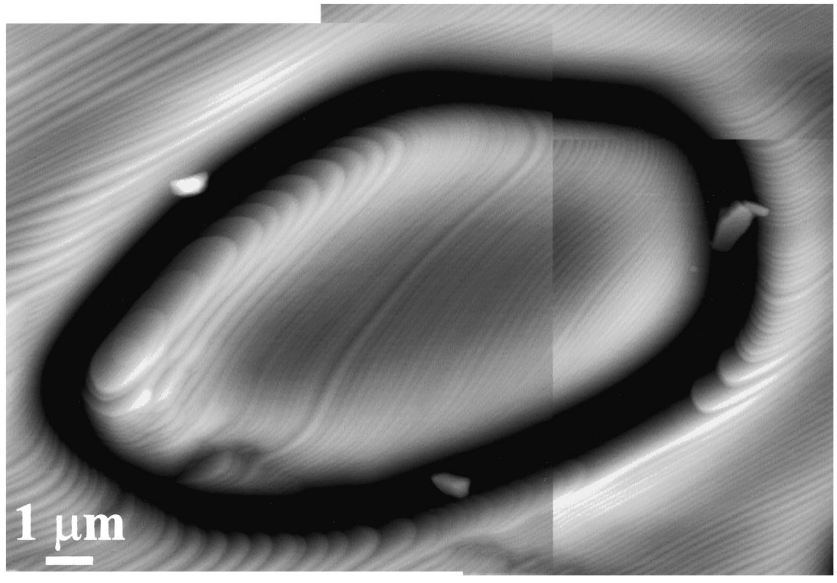

Fig. 2. Montage of AFM images showing an island grain. Black-to-white vertical contrast is 200 nm. Contrast discontinuities occur at the points where images have been pieced together. Surfaces are inclined from the ⟨111⟩ axis by ~10° and are slightly misoriented with respect to one another.

along the circumferences of G island grains, the total number of unknowns is $U = 2R(2R + 1) + G$. Because ~50 observations can be made at each island grain, an increment in G increases N much more than U. Thus, for even a few island grains, $N >> U$, and a set of best-fitted coefficients and grain-boundary energies can be determined using a conventional linear least-squares procedure.

The procedure described above should be widely applicable to most polycrystalline materials. It is not required that the island grains be completely isolated in the matrix grain, only that the observations be accumulated from a boundary with constant misorientation and a significant degree of curvature (so that surfaces with many distinct orientations are exposed at the groove root). In our experience, large curvature is typically observed at low-angle grain boundaries. In fact, all of the island grains identified as part of this study have misorientations of <7° and presumably have been formed when a higher-mobility grain boundary has swept past during the coarsening of the microstructure.

(2) Sample Preparation

Magnesia powder was formed by decomposing 99.7%-pure magnesium carbonate (Fisher Scientific Co., Pittsburgh, PA) at 997°C in air. Uniaxial compaction in a hot press at 1700°C for 1 h at 61 MPa produced a disk with a diameter of 50 mm and an average thickness of 1.5 mm. Specimens cut from this disk then were packed in a magnesia crucible with the parent powder and annealed for 48 h at 1600°C in air. At the end of this treatment, the specimens were translucent. The geometric measurements used to characterize the thermal groove and grain-boundary geometry required specimens that are flat and have two parallel faces. Appropriate surfaces were prepared using an automatic polisher (Model PM5, Logitech, Inc., Fremont, CA). The surfaces were initially lapped with a 9 μm alumina slurry, and the final polish was achieved using an alkaline (pH ~10) colloidal silica (0.05 μm) slurry. The flatness of the final surface was measured using an inductive axial movement gauge head with a resolution of 0.1 μm (TESR, Model TT22, Brown and Sharpe, Wixom, MI); surfaces were determined to be flat, within ±0.3 μm over lateral dimensions of 1 cm. The surface was thermally grooved by annealing it in air for 5 h at 1400°C. One of the assumptions that underpinned our measurement was that the groove morphology was determined at 1400°C and that it did not change in a significant way during cooling. Considering the fact that the lateral and vertical dimensions of the grooves and surface facets scaled with the annealing time and maintain constant dihedral angles, this appeared to be a satisfactory approximation. The average grain size of the sample was 109 μm. At this stage, one sample was analyzed for impurities. The sample contained 0.2% calcium, 0.02% aluminum, 0.03% iron, 0.02% silicon, and 0.03% yttrium.

After thermal grooving, many island grains were located, and optical micrographs were recorded. A thin, uniform layer (in a typical experiment, 6 ± 0.3 μm) then was removed by polishing, and the thermal groove treatment was repeated. The island grains that remained after polishing (some terminate in the removed layer) were characterized more completely, as described below.

(3) Crystallite Orientations

The orientations of the matrix and island grains were determined from electron backscattered diffraction patterns (EBSPs). The grooved samples were imaged (uncoated) using scanning electron microscopy (SEM; Model XL40, Philips, Eindhoven, The Netherlands). EBSPs were obtained at a specimen tilt of 70° by pointing the beam at the grain of interest in the spot mode. Patterns were indexed using ORIENTATION IMAGING MICROSCOPY software, version 2.6 (TexSEM Laboratories, Inc., Draper, UT), which returned a set of Euler rotation angles (ϕ_1, Φ, ϕ_2) relating the crystal reference frame to the sample reference frame. The absolute orientation of each grain was determined from three separate diffraction patterns recorded in the same grain.

(4) Surface Inclinations

The orientations of the free surfaces at the groove root were determined by combining topographic atomic force microscopy (AFM) data with the orientation data derived from the EBSPs. The AFM data were recorded using a stand-alone AFM (Model SAA-125, Digital Instruments, Santa Barbara, CA) positioned above the specimen mounted on an X–Y translation stage (Model TSE-150, Burleigh Instruments, Fishers, NY) capable of reproducibly positioning the specimen with 50 nm resolution. Silicon nitride cantilevers (Model LNP, Digital Instruments) were used as probes. AFM data were used to determine the partial dihedral angles (χ_1 and χ_2) and the angle τ between $\mathbf{e}_1$ and $\mathbf{v}$ (see Fig. 1).

The method for determining the partial dihedral angles has been described in detail in a previous paper.[16] Briefly, the width and depth of the groove are determined from AFM topographs. In general, the grooves are not symmetric; therefore, the groove width associated with a particular crystallite is assumed to be twice the distance from the topographic minimum at the groove root to the crest of the adjacent peak. The depth is the vertical distance from the minimum at the groove root to the crest of the adjacent peak. If we assume a quasi-static groove profile, it is possible to determine the inclination of the surface at the groove root from a measurement of the width and depth.[16] We have used the relationship between the width, depth, and inclination determined by Robertson.[17] Because the analytical form of the quasi-static groove profile is determined under the assumption that the surface energies are isotropic, there is an approximation implicit in this procedure. Based on earlier work, the systematic errors associated with the tip convolution effect for these relatively wide and shallow grooves should be negligible, and the standard deviation from random errors is estimated to be 1°.[18]

More-significant errors potentially resulted from sample positioning. Because the surface orientations were determined by combining AFM and SEM observations, it was important that the specimen reference frame be coincident with the reference frame of both microscopes. To assist with alignment, two of the lateral edges of the specimen were cut so that they formed a right angle with each other and the analysis surface. On each microscope stage, these external features were used to align the specimen. We estimated that the uncertainty in the orientation that results from indexing and specimen positioning errors was not greater than 5°.

Based on the AFM data, the normal of the surface at the groove root ($\mathbf{n}_i$) has the following components in the laboratory reference frame:

$$n_{i,1} = \cos \chi_i \cos \tau$$

$$n_{i,2} = \cos \chi_i \sin \tau$$

$$n_{i,3} = (-1)^i \sin \chi_i \tag{5}$$

where the subscript i refers to the surfaces labeled in Fig. 1. The normal vector $\mathbf{n}_1$ is defined as pointing into the crystal. In the crystal reference frame, the components of the surface normal (z_i) are specified according to the following transformation:

$$z_i = g_{ij} n_j \tag{6}$$

where g_{ij} is given by[19]

$$g(\phi_1, \Phi, \phi_2) = \begin{bmatrix} c\phi_1 c\phi_2 - s\phi_1 s\phi_2 c\Phi & s\phi_1 c\phi_2 + c\phi_1 s\phi_2 c\Phi & s\phi_2 s\Phi \\ -c\phi_1 s\phi_2 - s\phi_1 c\phi_2 c\Phi & -s\phi_1 s\phi_2 + c\phi_1 c\phi_2 c\Phi & c\phi_2 s\Phi \\ s\phi_1 s\Phi & -c\phi_1 s\Phi & c\Phi \end{bmatrix} \tag{7}$$

where c and s represent sine and cosine, respectively. Finally, the surface normals are transformed to a unit triangle of distinct orientations in cubic orientation space where the normal vector $\mathbf{n}'$ has the components z_i':

$$z_i' = M_{ik} z_k \tag{8}$$

The components of $\mathbf{n}'$ are permutations of the absolute values of z_i, such that $z_1' \geq z_2' \geq z_3'$, and the values of M_{ik} are 0, 1, or -1 and are assigned in the following way. If $z_i' \neq |z_k|$, then $M_{ik} = 0$. If $z_i' = |z_k|$, then $M_{ik} = 1$ for positive z_k, and $M_{ik} = -1$ for negative z_k. The surface energy is parameterized in terms of the spherical coordinates θ and φ; the relationship between these variables and the components of the surface normal are

$$\theta = \cos^{-1} z_1' \qquad \varphi = \tan^{-1} \frac{z_3'}{z_2'} \tag{9}$$

The torque terms in Eqs. (2) and (3) can be evaluated using the following expression:

$$\frac{\partial \gamma_i}{\partial \chi_i} = \frac{\partial \theta}{\partial \chi_i} \frac{\partial \gamma_i}{\partial \theta} + \frac{\partial \varphi}{\partial \chi_i} \frac{\partial \gamma_i}{\partial \varphi} \tag{10}$$

Analytical expressions for $\partial\gamma_i/\partial\theta$ and $\partial\gamma_i/\partial\varphi$ are easily obtained from Eq. (4). Although the terms $\partial\theta/\partial\chi_i$ and $\partial\varphi/\partial\chi_i$ can be derived exactly, for computational ease they have been approximated as difference quotients, $\Delta\theta/\Delta\chi_i$ and $\Delta\varphi/\Delta\chi_i$, calculated by dividing the change that occurs in θ or φ ($\Delta\theta$ or $\Delta\varphi$) as the surface normal vector is rotated through a small, fixed angle about $\mathbf{l}$, by the rotation angle ($\Delta\chi_i$). The values of $\Delta\theta$ and $\Delta\varphi$ have been determined using a rotation matrix with elements R_{ij}:

$$R_{ij} = \delta_{ij} \cos(\Delta\chi) - \varepsilon_{ijk} l_k \sin(\Delta\chi) + [1 - \cos(\Delta\chi)] l_i l_j \tag{11}$$

where l_i are the components of the vector $\mathbf{l}$, δ_{ij} the Kronecker delta, and ε_{ijk} the permutation tensor. The results of the fit are insensitive to choices of $\Delta\chi < 1°$.

(5) Boundary Inclinations

Optical micrographs of each island grain were recorded before and after a thin layer of the specimen was removed by polishing. The field of view for these micrographs included approximately 20 additional grains in the adjacent microstructure so that the relative lateral positions of the two images could be determined by visually maximizing the overlap of all the grain boundaries in the image. Based on measurements of the amount of material removed and the apparent lateral shift of the boundary between the two images, the inclination (α) at each point (P_i) was determined. Considering the magnitude of the vertical distance (6 ± 0.3 μm) and our estimated uncertainty in the lateral registry between the two layers (1.5 μm), we anticipated that the maximum uncertainty on α was ~14°. This was by far the most uncertain measurement in this experiment, and the impact of this error is described in the Discussion section.

(6) Fitting

The approximate expression for the surface energy (Eq. (4)) was substituted into Eqs. (2) and (3), and a standard linear least-squares procedure (LSFIT[20]) was used to determine the best-fitted values of the coefficients. The quality of the fit was assessed by the ratio (ρ) of the sum of the squares of the residuals to the difference between the number of equations and the number of free parameters. The results presented in the next section are based on fits to Eq. (2). Fits that included Eqs. (2) and (3) yielded qualitatively similar results, but the value of ρ was 5 times larger. Possible reasons for this are described in the Discussion section. The data set consisted of 269 observations from five island grains. If a series of order $R = 1$ is used, then $\rho = 6.76 \times 10^{-3}$. When the data set was randomly partitioned into two smaller segments, fitting to each segment led to almost identical results (within the standard deviation of the fit). When more terms were included in the series, there were additional oscillations in the function, and ρ decreased slightly. For example, when $R = 2$, $\rho = 5.47 \times 10^{-3}$. In this case, the ordering of the relative energies at the low index surfaces was the same as for the $R = 1$ fit. However, when the $R = 2$ function was fitted to the randomly partitioned data sets, the results differed from one another and from the results obtained using the complete data set. For this reason, we took the result from the $R = 1$ series to be the more reliable result.

(7) Orientation Stability

AFM images of the specimen revealed that the surfaces of some grains were faceted (for example, see Fig. 2), whereas others were smooth. The faceted surfaces always contained ridges formed by the intersection of two planes, but no corners. When the surface inclination changed, as it did near a thermal groove, the ridges exhibited smoothly curved edges. Thus, all missing surface orientations could be made up of two stable planes. To map the orientations that were stable or unstable with respect to faceting, AFM images were recorded of the surfaces of more than 100 grains whose orientations were previously determined based on EBSP data. If steps with heights >2.1 nm were observed (this corresponds to 5 times the lattice spacing), the grain was labeled as faceted. If no steps or steps less than this height were observed, the grain was labeled as smooth. We choose this arbitrary cutoff as a dividing line between discrete and continuum behavior by assuming that, for steps of this height, the interaction between individual atoms at the top and bottom of the facet was negligible.

III. Results

The best-fitted coefficients for the series in Eq. (4) are listed in Table I. Based on these values, we calculated the energies of the low-index planes to have the following relations:

$$\frac{\gamma_{110}}{\gamma_{100}} = 1.040 \pm 0.008$$

$$\frac{\gamma_{111}}{\gamma_{100}} = 1.072 \pm 0.010$$

The uncertainties in the values of the energy were determined from the variances and covariances of the fitted coefficients.[21] The maximum energy occurred at the (111) orientation and the minimum at (100). The functional dependence is illustrated in Fig. 3, where the value of the function at each observed orientation (Fig. 3(a)) and the energy contours (Fig. 3(b)) are plotted in a unit triangle of distinguishable orientations. The value of the surface energy function along the perimeter of the unit triangle is graphed in Fig. 4. The best-fitted grain-boundary energies for each of the island grains are listed in Table II. In each case, the energy is less than that of the (100) surface.

The orientation stability map is shown in Fig. 5. With the exception of two outliers and a small amount of overlap in the distributions, the faceted and smooth orientations are well separated. Based on these data, it seems that surface orientations near (100) and (111) are unstable with respect to faceting.

IV. Discussion

Ignoring relaxation effects, the relative surface energy of different crystallographic planes should scale with the broken bond

Table I. Best Fitted Coefficients for the Surface Energy Function

Coefficient	Value[†]
a_{10}	0.118 (60)
b_{10}	0.084 (36)
a_{11}	−0.130 (60)
b_{11}	−0.056 (34)
c_{11}	−0.100 (22)
d_{11}	−0.438 (12)

[†]Standard deviation in the last two digits is given in parentheses.

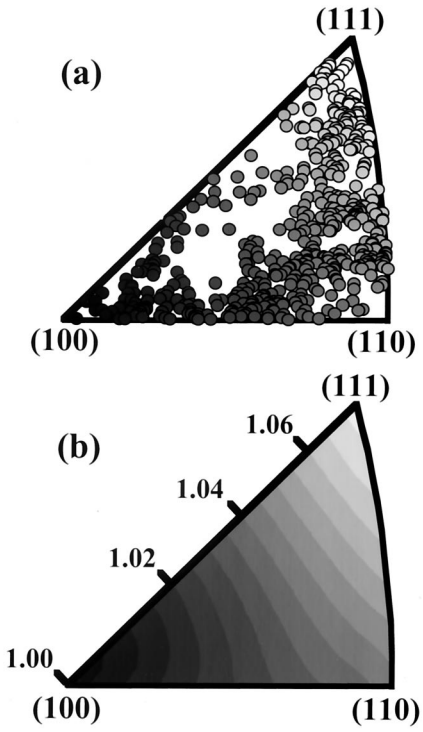

Fig. 3. (a) Orientations of surfaces at the groove roots of five island grains, plotted in a unit triangle of distinguishable orientations. Each point is shaded to represent the value of the best-fitted function at that point, where black corresponds to $\gamma_{hkl} = 1.000$ and white corresponds to $\gamma_{hkl} = 1.072$. (b) Surface energy contour plot constructed from the fitted function. Shading of the contours is the same as in (a).

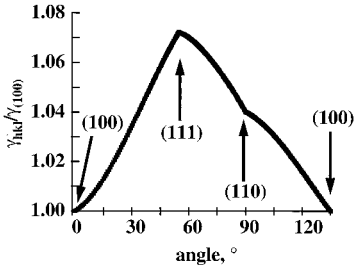

Fig. 4. Plot of the relative surface energy around the perimeter of the unit triangle, from (100) to (111), then to (110), and back to (100).

Table II. Best-Fitted Grain-Boundary Energies

Energy Relative to γ_{100}[†]	Misorientation (deg)	Axis
0.80 (1)	6.25	⟨0.99 0.13 0.06⟩
0.90 (1)	2.33	⟨0.79 0.61 0.04⟩
0.55 (2)	3.14	⟨0.69 0.68 0.28⟩
0.52 (2)	2.02	⟨0.81 0.58 0.02⟩
0.87 (2)	6.31	⟨0.92 0.33 0.20⟩

[†]Standard deviation in the last digit is given in parentheses.

density. Magnesia has the rock salt structure and only one bond per atom must be broken to create the (100) surface. Two and three bonds per atom must be broken to form the (110) and (111) surfaces, respectively. When the broken bond densities per unit area (σ) are compared, the (100) surface has the smallest value and $\sigma_{110}/\sigma_{100} = 2^{1/2}$ and $\sigma_{111}/\sigma_{100} = 3^{1/2}$. Therefore, the measured surface energies occur in the same order as the density of nearest-neighbor broken bonds on the surface. As expected, however, the measured variation in the energies in the real system (7%) is much less than that predicted by the simple bond-breaking

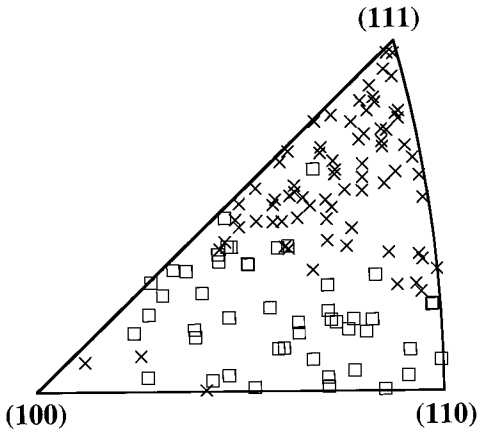

Fig. 5. Orientation stability map for magnesia at 1400°C. Each point corresponds to the orientation of an observed grain. Grains that are faceted are marked with an ×, and grains that are smooth are marked with an open square.

model. Anisotropies of 2%–8% have been previously observed in face-centered cubic (fcc) metals;[3–11] the current observations are consistent with the higher end of this range and less than the anisotropy reported for lithium fluoride (18%)[13] and sapphire (12%).[14]

The only previous experimental evaluation of the surface energy of magnesia was reported by Jura and Garland;[22] their calorimetric study of a fine powder led to the conclusion that the average surface energy of magnesia at room temperature is 1.0 J/m^2. Because the adsorption of water probably influenced this experiment, this value is likely to be an underestimate. There also have been model calculations of the surface energy of magnesia, and they are summarized in Table III.[23–27] With one exception, these studies place the energy of the (100) surface at ~1.0 J/m^2 at 0 K. Furthermore, in the cases where the energies of more than one surface have been computed, the energies have the same order as those observed in the present study ($\gamma_{100} < \gamma_{110} < \gamma_{111}$). The magnitude of the anisotropy predicted by these 0 K calculations is larger than experimentally observed and, in fact, is larger than it would be possible to observe in any equilibrium experiment. For example, if the energy of the (110) surface of a cubic crystal were $>2^{1/2}$ times the energy of the (100) surface, then the surface would lower its energy by faceting into (100) and (010) surfaces that would meet along lines in the [001] direction and form ridges. Therefore, the energy of the (110) orientation has an upper limit of $2^{1/2}\gamma_{100}$. Similarly, if the energy of the (111) surface were $>3^{1/2}$ times the energy of the (100) surface, it would lower its energy by faceting into trigonal pyramids bound by (100), (010), and (001) facets. Thus, the results of our experiments fall within the upper bounds set by the equilibrium condition.

A Wulff form was constructed based on the best-fitted energy function, and it is shown in Fig. 6. To construct the shape, orientation space was discretized (steps of 0.05 in k and l), and the surface energy of each orientation was assigned based on the best-fitted function. By applying the Wulff construction, a point on

Table III. Model Calculations of the Magnesia Surface Energy

Surface energy (J/m^2)				
(100)	(110)	(211)	(111)	Method[†]
1.16	2.92			Electrostatic model[21]
1.43				*Ab initio* Hartree–Fock LCAO[22]
1.07	2.78			Electrostatic model[23]
2.64			12.80	Harris–Foulkes functional (LDA)[24]
0.98	2.29	4.35		Self-consistent tight binding[25]

[†]LCAO is linear combination of atomic orbitals and LDA means local density approximation.

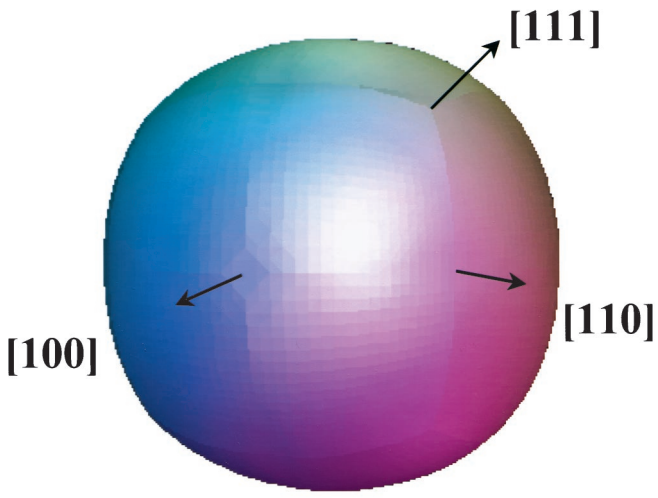

Fig. 6. Wulff shape of magnesia at 1400°C, determined from the fitted surface energy function.

the surface of the Wulff shape was found for each orientation. The space between each point then was filled in by QHULL and rendered in GEOMVIEW to create Fig. 6.[28]

Because of the discretization, continuously curved surfaces appear as regular arrays of flat squares visible in the detail of Fig. 6. There are, however, two other features that derive from the shape of the surface energy function. The first feature is the small flat facet at (100). Based on the extent of this facet, we conclude that {*hk*0} orientations inclined by $<5.7°$ from (100) are missing from the Wulff form. The second feature is the sharp edges formed by the intersections of the curved surfaces. These edges pass through (110) and meet at the (111) orientation. This means that orientations in the vicinity of the (111) orientation are missing and that the range of missing orientations extends toward the (110) orientation. It must be noted that the details of the Wulff form are extremely sensitive to the details of the energy function, which contains some uncertainty and is constrained by the choice of basis functions.[9] Increasing or decreasing the energies of selected orientations within the uncertainties of the function can affect the extent of the missing orientations in a significant way. However, we can test the validity of the Wulff form in Fig. 6 by comparing it with the orientation stability data.

The orientation stability figure presented in Fig. 5 indicates that surfaces inclined from (100) by $\leq 5°$ are unstable with respect to faceting. This result is consistent with the Wulff shape illustrated in Fig. 6, which shows that these orientations are missing from the equilibrium form. Orientations in the missing region break up into a (100) facet and a complex (high-index) facet $\sim 5°$ from (100). The specific index of the complex facet depends on the grain orientation. The angle at which the (100) plane intersects the complex surface can be used as an independent measure of the relative energy of the (100) plane (γ_{100}) and the complex plane (γ_c). When the Herring equilibrium condition is applied to the intersection of these two facets, we find that[2,15]

$$\frac{\gamma_{100}}{\gamma_c} = \cos \omega - \frac{1}{\gamma_c}\frac{\partial \gamma_c}{\partial \omega} \sin \omega \qquad (12)$$

Taking the second term in Eq. (12) to be negligible (for small ω, where ω is the angle between the surface normals), the relative energy is given by cos ω, which indicates that $\gamma_c/\gamma_{100} = 1.004$. This is consistent with the best-fitted surface energy function (see Fig. 4).

The faceted area near the (111) pole spans a much larger angular range than that near (100). Considering that the surface energy function maximizes at this orientation, we conclude that surfaces with these orientations facet to neighboring complex planes. The observation of faceting in this area is consistent with the Wulff shape, which shows curved surfaces meeting at sharp edges that intersect at {111} poles. The sharp edges on the Wulff shape occur when there are missing orientations; grains with such orientations may facet. The range of faceted orientations indicated in Fig. 5 appears to be larger than the range of missing orientations shown in Fig. 6. The observations also can be explained if the (111) orientation actually has a slightly lower energy than the surrounding orientations. In other words, within the uncertainty of the best-fitted function, it is possible that the surface energy maximum is inclined a few degrees from (111) and that the (111) orientation is a local minimum. If this were the case, then the orientations in the unstable region would always break up into a facet near (111) and a complex plane at the boundary between the smooth and faceted orientations. In principle, it should be possible to distinguish between these two scenarios by indexing the facets based on EBSP and AFM data. In this particular case, however, the small spacing of the facets makes their inclinations difficult to accurately quantify, and our measurements to date have led to ambiguous results. Although the ambiguous results most likely occur because of difficulties associated with the measurement, it is also possible that the shape of the energy function is more complicated than either of the two scenarios presented above.

The shape of the energy function that results from our fitting procedure is ultimately constrained by the number of harmonics used to approximate the energy. If complicated variations do occur, they are not reproduced by our function. However, the conclusion that the surface energy increases as the (111) orientation is approached is robust and consistent with theoretical predictions and earlier observations. The (111) surface of a compound with the rock salt structure is polar (terminated by ions with the same charge), and it has been argued that, because a polar surface has a dipole moment, its energy is always larger than the energies of other surfaces of the same solid that are either charge neutral or charged, but lacking a dipole moment.[29] The conventional view is that orientations vicinal to a low-index plane have relatively higher energies, because additional bonds must be broken to create a terrace–step structure. However, this rational does not necessarily apply to a polar surface. In this case, although the step creation does break additional bonds, it also introduces ions of the opposite sign, and this reduces the surface charge imbalance. For example, adjacent (111) terraces of the rock salt structure separated by monoatomic steps are terminated by ions of opposite charge. Thus, a decrease in the surface energy with step density can occur if the gain in electrostatic stability is greater than the cost of breaking bonds to create steps.

Earlier experimental studies of magnesia surfaces have been conducted in temperature ranges above and below the current study (but at different partial pressures of oxygen). For example, Henrich[30] annealed an ion-bombarded magnesia (111) surface under ultrahigh vacuum to temperatures as high as 1127°C and found that the surface faceted into trigonal pyramids bounded by (100) planes. This would imply a higher degree of anisotropy than what we have observed, which would be consistent with the lower temperatures used for the annealing. When the magnesia (111) surface was examined by reflection electron microscopy after being annealed at 1550°–1700°C in oxygen, it was found to be smooth (but reconstructed on the atomic scale) and stable against faceting.[31] Although the widely different partial pressures of oxygen used in the aforementioned studies might make a rigorous comparison inappropriate, the transition from a faceted surface at 1127°C[30] to a partially faceted surface at 1400°C (the current study) and to a smooth surface at 1500°C[31] is consistent with the reduction in anisotropy that is expected at elevated temperatures. In fact, this transition might be analogous to that observed in the isostructural compound halite, for which smooth (111) surfaces are observed only above 650°C.[32] In the present and previous studies, calcium was the major impurity, and this is known to segregate to the surface.[33] Reflection electron microscopy experiments have shown that the step structure on the (100) surface can be altered by calcium segregation;[34] therefore, we must conclude that the exact form of the surface energy function is sensitive to the temperature and partial pressure of oxygen, and to the concentration of dissolved (and segregated) impurities.

The best-fitted grain-boundary energies (see Table II) are all less than the surface energy. The median grain boundary to surface energy ratio has been previously measured to be 1.2, which indicates that most of the grain boundaries in a random polycrystal have an energy that is greater than the surface energy.[16,35] The distribution of energy ratios, however, extends as low as 0.65 for low-angle boundaries.[16] Therefore, the low energies that result from our fit are not surprising, considering that the largest misorientation is $<7°$. With one exception, the fitted grain-boundary energy increases with the misorientation angle. Although the exception might be due to experimental error, it is probably not appropriate to establish a correlation between the grain-boundary energy and only one of the five macroscopic degrees of freedom that define the grain-boundary character.

One of the assumptions applied in our analysis is that the grain-boundary energy is independent of the boundary plane. In other words, the energy of the grain boundary at all points around the thermal groove is assumed to be the same. If the best-fitted surface energy function is used to determine the energies of the surfaces bounding the groove at each point around an island grain's circumference, the Herring[15] equilibrium condition can be used to compute a boundary energy at each point. Energies computed in this way vary systematically with position and suggest that the boundary plane does influence the grain-boundary energy. That we average over these variations in our fitting procedure (and ignore the grain-boundary torque terms) is one of the sources of uncertainty in our result.

Finally, Eq. (3) has been neglected in our fitting procedure. In earlier work, Eq. (3) has been ignored without comment.[3–9] Including Eq. (3) in the procedure described here increases the uncertainty in the result. The reason for this is evident when we compare the form of the equations. In Eqs. (2) and (3), the magnitude of the left-hand side is determined by α, a measured parameter that is typically near zero (78% of the observations are in the range $-20° < \alpha < 20°$) and contains the highest degree of experimental uncertainty. The left-hand side of Eq. (2) scales with $\cos \alpha$, and the left-hand side of Eq. (3) scales with $\sin \alpha$, so that, when α is small, measurement errors are magnified by Eq. (3) and diminished by Eq. (2). For example, a 15° error in the measurement of $\alpha \approx 0$ leads to an uncertainty on the left-hand side of Eq. (2) of 3.5%; for Eq. (3), the same error leads to an uncertainty of 26%.

An alternate approach to reconstructing the surface energy function from thermal groove data, which considers both components of Eq. (1), is described in the forthcoming paper.[36] This new method is statistical in nature, multiscale in implementation, and affords efficient incorporation of the full vector equilibrium equation. Other main advantages in this approach include no a priori basis selection for the surface energy representation and efficient accommodation of large amounts of experimental data.

V. Conclusions

An experimental technique has been developed to determine the anisotropy of surface energy. The technique uses polycrystalline specimens and is based on the analysis of crystallographic data obtained from EBSPs and geometric data obtained by AFM. We have tested the method on magnesia and found that, at 1400°C, $\gamma_{110}/\gamma_{100} = 1.040 \pm 0.008$ and $\gamma_{111}/\gamma_{100} = 1.072 \pm 0.010$. The surface energy minimum is at (100), and this leads to the faceting of orientations within 5° of this surface. The surface energy maximum occurs at or very near the (111) orientation, which is a polar surface. An orientation stability map indicates that orientations near (111) are unstable with respect to faceting. It should be possible to conduct similar measurements on any polycrystalline specimen that has a grain size >30 μm and contains some enclosed or partially enclosed grains.

References

[1]A. J. W. Moore, "The Influence of Surface Energy on Thermal Etching," *Acta Metall.*, **6** [4] 293–304 (1958).

[2]A. J. W. Moore, "Thermal Faceting"; pp. 155–98 in *Metal Surfaces: Structure, Energetics, and Kinetics*. Edited by N. A. Gjostein and W. D. Robertson. American Society for Metals, Metals Park, OH, 1963.

[3]H. Mykura, "The Variation of the Surface Tension of Nickel with Crystallographic Orientation," *Acta Metall.*, **9** [6] 570–76 (1961).

[4]W. M. Robertson and P. G. Shewmon, "Variation of the Surface Tension with Orientation in Copper," *Trans. Metall. Soc. AIME*, **224** [4] 804–11 (1962).

[5]M. McLean and H. Mykura, "The Orientation Dependence of Surface Tension for Face-Centered-Cubic Iron," *Acta Metall.*, **12** [3] 326–28 (1964).

[6]W. A. Winterbottom and N. A. Gjostein, "Determination of the Anisotropy of Surface Energy of Metals—I: Theoretical Analysis," *Acta Metall.*, **14** [9] 1033–40 (1966).

[7]W. A. Winterbottom and N. A. Gjostein, "Determination of the Anisotropy of Surface Energy of Metals—II: Experimental γ-Plot of Au," *Acta Metall.*, **14** [9] 1041–52 (1966).

[8]M. McLean and B. Gale, "Surface Energy Anisotropy by an Improved Thermal Grooving Technique," *Philos. Mag.*, **20** [167] 1033–45 (1969).

[9]B. Gale, R. A. Hunt, and M. McLean, "An Analysis of Surface Energy Anisotropy Data Using Lattice Harmonics," *Philos. Mag.*, **25** [4] 947–60 (1972).

[10]J. C. Heyraud and J. J. Métois, "Equilibrium Shape and Temperature; Lead on Graphite," *Surf. Sci.*, **128** [2/3] 334–42 (1983).

[11]J. C. Heyraud and J. J. Métois, "Equilibrium Shape of Gold Crystallites on a Graphite Cleavage Surface: Surface Energies and Interfacial Energy," *Acta Metall.*, **28** [12] 1789–97 (1980).

[12]R. S. Nelson, D. J. Mazey, and R. S. Barnes, "The Thermal Equilibrium Shape and Sizes of Holes in Solids," *Philos. Mag.*, **11** [109] 91–111 (1965).

[13]Z. Y. Wang, M. P. Harmer, and Y. T. Chou, "Pore–Grain Boundary Configurations in Lithium Fluoride," *J. Am. Ceram. Soc.*, **69** [10] 735–40 (1986).

[14]J.-H. Choi, D.-Y. Kim, B. J. Hockey, S. M. Wiederhorn, C. A. Handwerker, J. E. Blendell, W. C. Carter, and A. R. Roosen, "Equilibrium Shape of Internal Cavities in Sapphire," *J. Am. Ceram. Soc.*, **80** [1] 62–68 (1997).

[15]C. Herring, "Surface Tension as a Motivation for Sintering"; pp. 143–79 in *The Physics of Powder Metallurgy*. Edited by W. E. Kingston. McGraw-Hill, New York, 1951.

[16]W. W. Mullins, "Theory of Thermal Grooving," *J. Appl. Phys.*, **28** [3] 333–39 (1957).

[17]W. M. Robertson, "Grain-Boundary Grooving by Surface Diffusion for Finite Surface Slopes," *J. Appl. Phys.*, **42** [1] 463–67 (1971).

[18]D. M. Saylor and G. S. Rohrer, "Measuring the Influence of Grain-Boundary Misorientation on Thermal Groove Geometry in Ceramic Polycrystals," *J. Am. Ceram. Soc.*, **82** [6] 1529–36 (1999).

[19]H.-J. Bunge, *Texture Analysis in Materials Science*; p. 21. Translated by P. R. Morris. Butterworths, London, U.K., 1982.

[20]W. H. Press, B. P. Flannery, S. A. Teukolsky, and W. T. Vetterling, *Numerical Recipes in Pascal*; pp. 563–65. Cambridge University Press, Cambridge, U.K., 1989.

[21]G. W. Snedecor and W. G. Cochran, *Statistical Methods*, 7th ed.; p. 342. Iowa State University Press, Ames, IA, 1980.

[22]G. Jura and C. W. Garland, "The Experimental Determination of the Surface Tension of Magnesium Oxide," *J. Am. Chem. Soc.*, **74** [4] 6033–34 (1952).

[23]P. W. Tasker and D. M. Duffy, "The Structure and Properties of the Stepped Surfaces of MgO and NiO," *Surf. Sci.*, **137** [1] 91–102 (1984).

[24]M. Causa, R. Dovesi, C. Pisani, and C. Roetti, "*Ab Initio* Hartree–Fock Study of the MgO(001) Surface," *Surf. Sci.*, **175** [3] 551–60 (1986).

[25]W. C. Mackrodt, "Atomistic Simulation of Oxide Surfaces," *Phys. Chem. Miner.*, **15** [3] 228–37 (1988).

[26]A. Gibson, R. Haydock, and J. P. LaFemina, "Electronic Structure and Relative Stability of the MgO(001) and (111) Surfaces," *J. Vac. Sci. Technol. A*, **10** [4] 2361–66 (1992).

[27]J. Goniakowski and C. Noguera, "Electronic Structure of Clean Insulating Oxide Surfaces I. A Numerical Approach," *Surf. Sci.*, **319** [1/2] 68–80 (1994).

[28]QHULL and GEOMVIEW are public domain software made available by the Geometry Center, Minneapolis, MN, at http://www.geom.umn.edu/.

[29]P. W. Tasker, "The Stability of Ionic Crystal Surfaces," *J. Phys. C: Solid State Phys.*, **12** [22] 4977–84 (1979).

[30]V. E. Henrich, "Thermal Faceting of the (110) and (111) Surfaces of MgO," *Surf. Sci.*, **57** [1] 385–92 (1976).

[31]M. Gajdardziska-Josifovska, P. A. Crozier, and J. M. Cowley, "A $(\sqrt{3}\times\sqrt{3})$R30° Reconstruction on Annealed (111) Surfaces of MgO," *Surf. Sci. Lett.*, **248** [1/2] L259–L264 (1991).

[32]J. C. Heyraud and J. J. Métois, "Equilibrium Shape of an Ionic Crystal in Equilibrium with its Vapour (NaCl)," *J. Cryst. Growth*, **84** [3] 503–508 (1987).

[33]R. C. McCune and P. Wynblatt, "Calcium Segregation to a Magnesium Oxide (100) Surface," *J. Am. Ceram. Soc.*, **66** [2] 111–17 (1983).

[34]M. Gajdardziska-Josifovska, P. A. Crozier, M. R. McCartney, and J. M. Cowley, "Ca Segregation and Step Modifications on Cleaved and Annealed MgO(100) Surfaces," *Surf. Sci.*, **284** [1/2] 186–99 (1993).

[35]C. A. Handwerker, J. M. Dynys, R. M. Cannon, and R. L. Coble, "Dihedral Angles in Magnesia and Alumina: Distributions from Surface Thermal Grooves," *J. Am. Ceram. Soc.*, **73** [5] 1371–77 (1990).

[36]D. E. Mason, D. Kinderlehrer, and I. Livshits, "The Surface Energy of Magnesia: Multiscale Reconstruction from Thermal Groove Geometry," unpublished work. □